SEMARAK ILMU PUBLISHING

Journal of Advanced Research in Fluid Mechanics and Thermal Sciences

Journal homepage:
https://semarakilmu.com.my/journals/index.php/fluid_mechanics_thermal_sciences/index
ISSN: 2289-7879

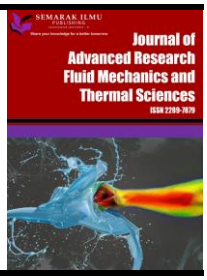

Effect of Cross-Sectional Depth on Horizontal and 30° Slop Spillway Open Channel Pico Hydro Cross-Flow Turbine Efficiency

Aji Putro Prakoso[1,2,*], Budiarso[1], Warjito[1], Ahmad Fudholi[3,4], Deny Bayu Saefudin[2], Chairul Umam Rosyadi[2], Aris Suryadi[5], Ghalya Fikra[6], Yadi Radiansyah[3], Yusuf Suryo Utomo[3]

[1] Department of Mechanical Engineering, Faculty of Engineering, Universitas Indonesia, Indonesia
[2] Mechanical Engineering Program, Faculty of Manufacturing Technology, Universitas Jenderal Achmad Yani, Indonesia
[3] Research Center for Energy Conversion and Conservation, National Research and Innovation Agency (BRIN), Indonesia
[4] Solar Energy Research Institute, Universiti Kebangsaan Malaysia, Malaysia
[5] Electrical Technology Program, Politeknik Enjinering Indorama Purwakarta, Indonesia
[6] Research Center for Intelligent Mechatronics, National Research and Innovation Agency (BRIN), Indonesia

ARTICLE INFO

Article history:
Received 5 October 2023
Received in revised form 22 December 2023
Accepted 4 January 2024
Available online 15 January 2024

Keywords:
Open channel flow; spillway; pico hydro; turbine; cross-flow; depth

ABSTRACT

Harvesting the kinetic energy from the small dam's spillway downstream flow in agricultural areas is interesting. On the other hand, a cross-flow turbine (CFT) is a unique impulse turbine because it works at a higher specific speed, which means this turbine works at a lower head and higher water flow rate. Thus, there is an opportunity to use a CFT to harvest the energy in the spillway. There are two possible scenarios: at the flat horizontal and the 30° slop flow. Several computational fluid dynamics (CFD) simulations were conducted to test the hypothesis. The simulations were performed with five variations of the ratio between the cross-sectional depth parameter of the spillway's flow before approaching the turbine for each scenario. The total head in the present study case is 3.0 meters with 120 l/s of water discharge. The simulations used ANSYS® Fluent™ for 2D CFD simulation. The tests found that the CFT could attain 80.36% efficiency. Moreover, some water flows over the turbine at a higher rotational speed, leading to a significant loss in turbine performance, called potential loss. This finding indicates that the CFT could harvest the spillway's flow kinetic energy when the flow is not too deep.

1. Introduction

A small dam crossing the river flow is one essential building in agricultural areas [1]. Dams are critical for raising the water level higher than the ground and distributing it into landfills [2]. The raised water level upstream of the dam generates kinetic energy at the downstream flow of the irrigation dam's spillway [3]. This kinetic energy inside the water is attractive for utilization as electricity.

Harvesting the water's kinetic energy on the spillway is challenging because no machine suits this flow type. All waterwheels work for open channel flow (OCF), but they mainly utilize water's potential

* *Corresponding author.*
E-mail address: ajipp13@gmail.com

https://doi.org/10.37934/arfmts.113.1.176187

energy directly from the water's weight or by damming up the flow [4,5]. Before approaching the breastshot and undershot waterwheel, the increased water kinetic energy will not escalate their performance [6,7]. On the other hand, impulse turbines, e.g., Pelton turbine, Turgo turbine, and cross-flow Banki turbine (CFT), generate water's kinetic energy using a nozzle connected to the pipeline, not an OCF [8]. However, the CFT nozzle is a rectangular planar-symmetrical channel identical to water inside a rectangular cross-section (RCS)-OCF [9].

The similarity between RCS-OCF and CFT nozzles leads Prakoso *et al.,* [10] to introduce a hydrokinetics CFT, which works at a tiny head jump without a nozzle in an RCS-OCF. However, the CFT performance in that study was unsuitable due to the angle-of-attack disuniformity between the water's and the turbine's tip velocity. Prior studies about spillway flow CFT have already been conducted for the spillway's slop angle and the CFT blade's profile parameters [10,11]. The first study found that the 30° slope spillway leads to the best OCF-CFT performance. That result might be influenced by the slope angle or the relative turning angle before the turbine. A further one found that a non-airfoil-based blade profile still performs better than the airfoil-based blade profile in OCF-CFT. The results indicate that the impulse behaviour still exists in this type of pico hydro turbine. However, those studies still have not optimized the RCS depth for the spillway OCF. In contrast, the cross-sectional (CS) depth is a crucial parameter influencing the mean velocity and the maximum discharge capacity for an OCF-CFT.

2. Methodology

This study uses several computational fluid dynamics (CFD) numerical simulations to find the optimum CS depth for OCF-CFT. The simulations tested the CFT works on five CS depth cases in a horizontal and 30° slop spillway condition. The horizontal RCS-OCF is still maintained in this study to find the opportunity for OCF-CFT to be applied not only on an embankment dam but also on a high-speed OCF after a sluice gate. The total head jump in this study is set at three meters for both discussed scenarios. The CFT tested in this study has a 160 mm outer diameter, similar to several prior studies, to make this study's results more comparable [10-13]. Based on Sammartano's inlet velocity equation, this study's CFT working speed is predicted to be about 440 RPM [14]. Moreover, for pico hydro scale application, the CFT in this study works at about 3.5 kW of water's potential power and 120 l/s discharge capacity. Thus, this turbine works at specific-speed (N_s) of 56. The CFT whole design and the CFD cases are reported in Chapter 2.1 of this paper.

2.1 CFD Simulations Cases

This paper's CFT impeller design methodology refers to the optimized design parameters for nozzle-based CFT investigated in the prior study [12]. However, some adaptations and assumptions exist for the RCS-OCF parameters and behaviours regarding the CFT nozzle design. The design parameters for this study's CFT impeller can be seen in Table 1. Moreover, based on the nozzle initial height equation mentioned in prior works, assuming that there are no hydraulic jumps before entering the turbine and the angle of attack (α) is 22°, the relationship between the ratio of initial height and outer diameter ($^{S_0}/_{D}$) with the nozzle exit width angle (λ) obey Eq. (1) [12].

$$^{S_0}/_{D} = 0.1873\lambda \tag{1}$$

While λ in the OCF case in this study, it can be interpreted as the water entrance width angle in radians unit. However, based on two prior studies, the no-hydraulic-jump assumption was not valid, especially at higher rotational speeds. The hydraulic jump was formed due to the centrifugal force effects found in CFT since 1960 [15]. In a nozzle-equipped CFT, the centrifugal force effect generates the nozzle velocity coefficient investigated in a prior study and is valued between 0.9 and 1 [14].

Table 1
CFT impeller design parameters [11-13]

Parameter (Symbol) [Unit]	Value	Parameter (Symbol) [Unit]	Value
Outer diameter (D) [m]	0.160	Blade's outlet angle (β_2) [°]	90
Inner diameter (d) [m]	0.104	Blade's radius (R_b) [m]	0.030
O-I diam. ratio ($^{d}/_{D}$)	0.65	Blade's radius ratio ($^{R_b}/_{D}$)	0.187
Angle of attack (α) [°]	22	Blade's curve angle (δ_b) [°]	60
Blade's inlet angle (β_1) [°]	39	Blade's number (N_b)	35

The mentioned hydraulic jump phenomenon leads to the difficulty of OCF cross-sectional depth (d_C) calculation. Usually, based on Eq. (1), the nozzle inlet ratio for $\lambda = {}^{\pi}/_{2}$ estimated at 0.2942, while the d_C value in this study varies from 0.0625 to 0.3125 with a 0.0625 increment. The prior study found that the water's velocity distribution approaching the turbine affects the turbine's performance [16]. On the other hand, the OCF velocity distribution is different from the in-nozzle velocity distribution and the inviscid approach. The inlet location is located $2.5D$ away from the turbine to ensure that the OCF velocity profile is fully developed before approaching the turbine. This distance is provenly adequate to have an identical velocity profile with the experiment results of the OCF velocity profile in a previous study [11,17,18].

Moreover, the distance between the turbine and the outer boundary has a minimum space of $1.5D$, which is stated as the air pressure outlet. Then, the border below the turbine is expressed as a water pressure outlet located only 1 cm from the turbine's sheath. The drawing in Figure 1 represents the simulation case for horizontal and 30° slop spillway conditions.

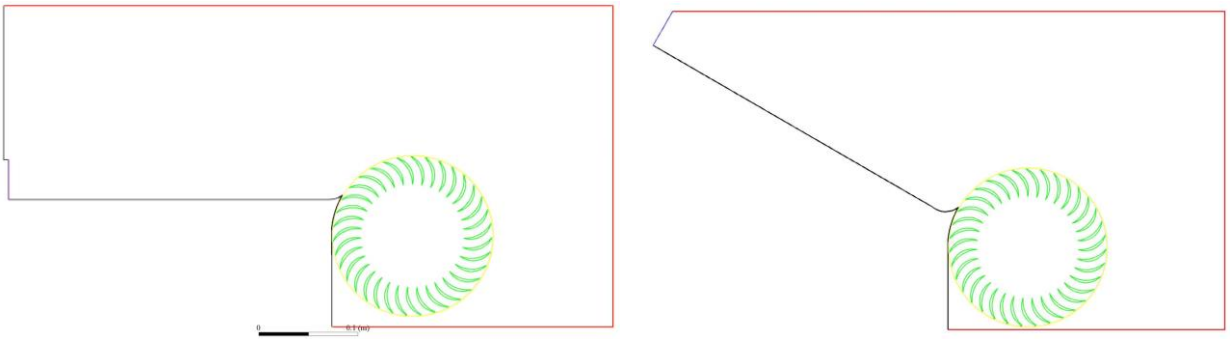

(a) (b)

Fig. 1. CFD Simulation cases: (a) Horizontal case, (b) 30° slop case

2.2 CFD Simulations Process

This study uses the academic version ANSYS Fluent 18.1 for the CFD simulation tests. The difference between the academic and commercial versions is that the educational version mesh elements and nodes couldn't exceed 500,000. However, as this study's simulation case is tested in planar-symmetry 2D simulation, the mesh elements and nodes' number never exceed 100,000 for good enough simulation.

The CFD simulations in this study are generally divided into four big stages: meshing, setups, solving, and post-processing. The meshing stage is started by specifying the mesh sizing for the CFD cases. Even though this is the first step in a CFD simulation, it is crucial to attaining a good simulation result. A small change in the mesh size setting could affect the mesh element number and skewness change. After the mesh size is set, the mesh grid can be generated from the simulation case. Then, the grid generation result skewness must be checked before proceeding to the next step. The accepted mesh for an accurate CFD simulation is when the maximum skewness value does not exceed 0.9. If the skewness value is still below the limit, the next step is to ensure the CFD computational result is not affected by the mesh elements's number change. The method used uses GCI values as the results of the Richardson extrapolation method. The GCI value is the logarithmic-normalized value of the error test variable in one number of mesh elements to the inversed-exponential-extrapolation approximation result [19]. Previous studies have reported the Richardson extrapolation steps and implementation used in this study [10,20]. The adequate number of mesh elements results in less than 1% GCI by several systematic trial and error methods [13]. The last step in the meshing stage is naming the boundaries as inlet, outlet, blades, and interfaces before being automatically exported to the Fluent meshing format.

The second stage of the CFD simulation is the setup stage. This stage mainly involves setting up the imported case with governing equations, boundary conditions, and solving methodology. The volume of fluid multiphase equations in this simulation is turned on.

Prior studies recommend the two-equations RNG k-ε turbulence model compared to the standard two-equations k-ε and the two-equations SST k-ω model for the CFT CFD simulations due to its accuracy among [21,22]. However, the recently founded four-equations Transitional SST turbulence model is more promising, with a competitive accuracy and ability to quickly converge the iteration process based on other previous studies [13,14]. Therefore, this study uses the four-equations Transitional SST turbulence model. The four equations used in the Transitional SST model consist of two equations from the SST k-ω model, the intermittency (Γ) equation, and the average momentum Reynolds thickness ($\widetilde{Re}_{\theta t}$) equation. Those equations are then used to find the turbulence kinetic energy (k) and turbulence viscosity (μ_t) values, which are crucial to solving the Boussinesq Equation in Eq. (2).

$$-\rho\overline{u`_i u`_j} = \mu_t\left(\frac{\partial u_i}{\partial x_j}+\frac{\partial u_j}{\partial x_i}\right) - {}^2/_3\left(\rho k + \mu_t \frac{\partial u_k}{\partial x_k}\right)\delta_{ij} \tag{2}$$

The lefthand parameter in the Boussinesq Equation is the turbulence shear stress variable. This variable is the primary parameter in a turbulence flow. Moreover, the velocity distribution regarding turbulence shear stress can be solved using the Reynolds Averaged Navier-Stokes (RANS) equation in Eq. (3).

$$\frac{\partial}{\partial t}(\rho u_i) + \frac{\partial}{\partial x_j}(\rho u_i u_j) = -\frac{\partial p}{\partial x_j} + \frac{\partial}{\partial x_j}\left(\mu_t\left(\frac{\partial u_i}{\partial x_j}+\frac{\partial u_j}{\partial x_i} - {}^2/_3\,\delta_{ij}\frac{\partial u_l}{\partial x_l}\right)\right) + \frac{\partial}{\partial x_j}\left(-\rho\overline{u`_i u`_j}\right) \tag{3}$$

This study uses velocity inlet for the inlet boundary condition (BC), pressure outlet for the outlet BC, and moving wall for blade BC. The velocity value for the inlet BC is calculated based on the head of the inlet location using Eq. (4). The relative static pressure for the outlet BC is stated as 0 Pa. Moreover, this study uses the sliding mesh method with a rotational speed equal to the moving wall condition.

$$\bar{V}_{inlet} = \sqrt{2g(H - H_{inlet})} \quad (4)$$

To solve the problems in this study case, this study uses the second-order upwind discretization scheme and bounded second-order implicit time discretization method. The coupled pressure-velocity calculation scheme with the body-force weighted pressure discretization scheme is also used in this simulation. The autosave option is turned on during the numerical calculation for every 100 timesteps, and then, the automatic export to CFD-Post format is enabled for every two timesteps. The initial value for the computational iteration is set from the inlet with 0 m/s of initial velocity, 0.1 m^2/s^2 of turbulence kinetic energy, 10 m^2/s^3 of eddy dissipation rate, and 122 of momentum Re thickness. These simulations run for 800 timesteps with 0.0005 s of timestep size. The value of the timestep size has been tested with the Courant number equation stated in Eq. (5), with the result being $Cr \approx 0.88$, which is acceptable because it is below one. Moreover, the simulation uses a maximum of 200 iterations for each time step.

$$Cr = \frac{u_{max} \cdot \Delta t}{\Delta x} \quad (5)$$

The next stage of the simulation process is the solving stage based on the specifications set in the setup stage. However, this study uses 10^{-4} residual convergency criteria to ensure precise enough calculation results. This study also uses double-number precision, meaning the calculation uses 64-bit number representation, which is also recommended for transient multiphase simulations.

The final stage is the post-processing stage, which generates understandable data from big numerical data produced during the solving phase. The exported data from the post-processing software are usually vector plots, contour plots, charts, and tables. The exported data is then manually processed before being compared and verified with prior studies' findings or theoretical approach data. When the simulation results are understandable, reasonable, and convincing enough, the simulation results are discussed to produce this study's conclusion. The summary of the simulation process can be seen in Figure 2.

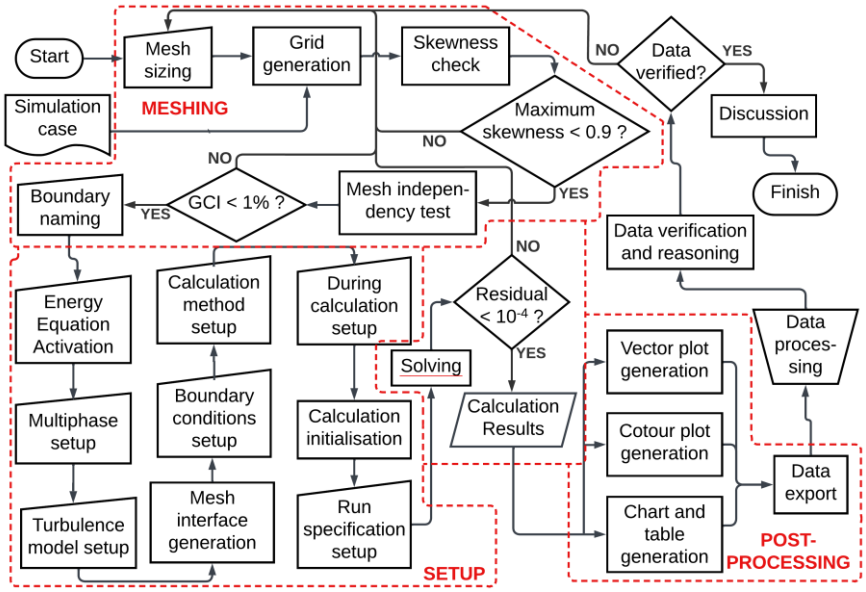

Fig. 2. CFD Simulation process flowchart

3. Results

Some results from several simulations are reported in this chapter. The first report is about the mesh independence test process before the main simulations are conducted. Then, the CFT power and efficiency were reported, followed by the spillway OCF CS depth optimization for horizontal and 30° conditions.

3.1 Mesh Independence Test Results

This study varied the mesh elements' number in four values: 6.5k, 13k, 26k, and 52k elements in a 30° slop case for the mesh independence test. Then, the same mesh sizing settings are used for the horizontal channel case. The independence test finds that the results of the GCI calculation with a total of 26k elements, a good Grid Convergence Index (GCI) value of 0.83%, is obtained because this value does not exceed 1%, so the resulting mesh quality is good and acceptable. Thus, this study's CFD simulations use mesh size settings similar to the 26k mesh elements. The sizings are 5 mm for the general sizing, 2.5 mm for the open channel, inlet and outlet boundaries, 2.5 mm for the rotating elements inside and around the CFT, 1.2 mm for the 'blades' boundary, and 0.5 mm for the inner and outer interface boundaries. Moreover, the overall independence test results can be found in Table 2. This simulation mesh visualization can be seen in Figure 3.

Table 2
Mesh independence test results

Elements' number	Refinement ratio	No rotation torque	Convergent order	Extrapolated torque value	GCI
6.5k	-	145.92	-		2.50%
13k	1.41	144.58	-3.6	143.348	1.20%
26k	1.41	144.2	-3.6	143.348	0.83%
52k	1.41	143.59	-		0.24%

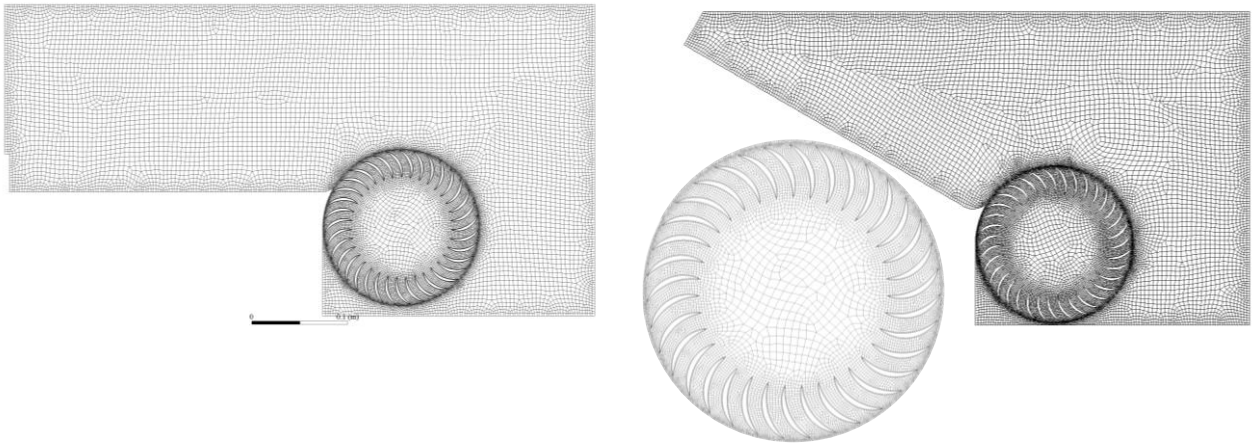

(a) (b)

Fig. 3. The CFD simulation mesh visualization: (a) Horizontal case, (b) 30° slop case

3.2 The CFT Power and Efficiency

This study found that the maximum CFT power attained from a horizontal flow OCF-CFT is 971 Watts, while at the 30° slop spillway condition, the OCF-CFT can gain 958 Watts. The maximum power

in both scenarios is attained at 300 RPM rotation speed and $^{d_c}/_{D} = 0.25$ condition. Moreover, the highest efficiency is attained on 30° slop conditions at 400 RPM and $^{d_c}/_{D} = 0.1825$. The maximum efficiency at this point is 80.36%, but the horizontal spillway condition also gains a good efficiency of about 77.58%. This efficiency is found at the same speed but at $^{d_c}/_{D}$ about 0.125. The charts in Figure 4(a) and Figure 4(b) show the overall power and efficiency results.

3.3 The Optimum $^{d_c}/_{D}$ Condition

This study approximates the maximum power and efficiency for each case previously obtained by CFD simulations by utilizing the least-square data fit for a parabolic curve. The maximum efficiency is then plotted into an efficiency versus $^{d_c}/_{D}$ chart, which can be seen in Figure 4(c). From Figure 4(c), it can be seen that the optimum $^{d_c}/_{D}$ for the horizontal flow condition is 0.125, and it is expected to produce 72.8% of efficiency. Moreover, the 30° slop spillway case can attain the optimum efficiency at 81.7% with $^{d_c}/_{D} = 0.8175$. An interesting thing to note is that the optimum $^{d_c}/_{D}$ for horizontal and 30° slop spillway conditions are different. Further study is needed to find the optimum $^{d_c}/_{D}$ for other spillway slop conditions, such as 45° and 60°, to find the pattern or relation between the slop angle and the optimum CS depth ratio.

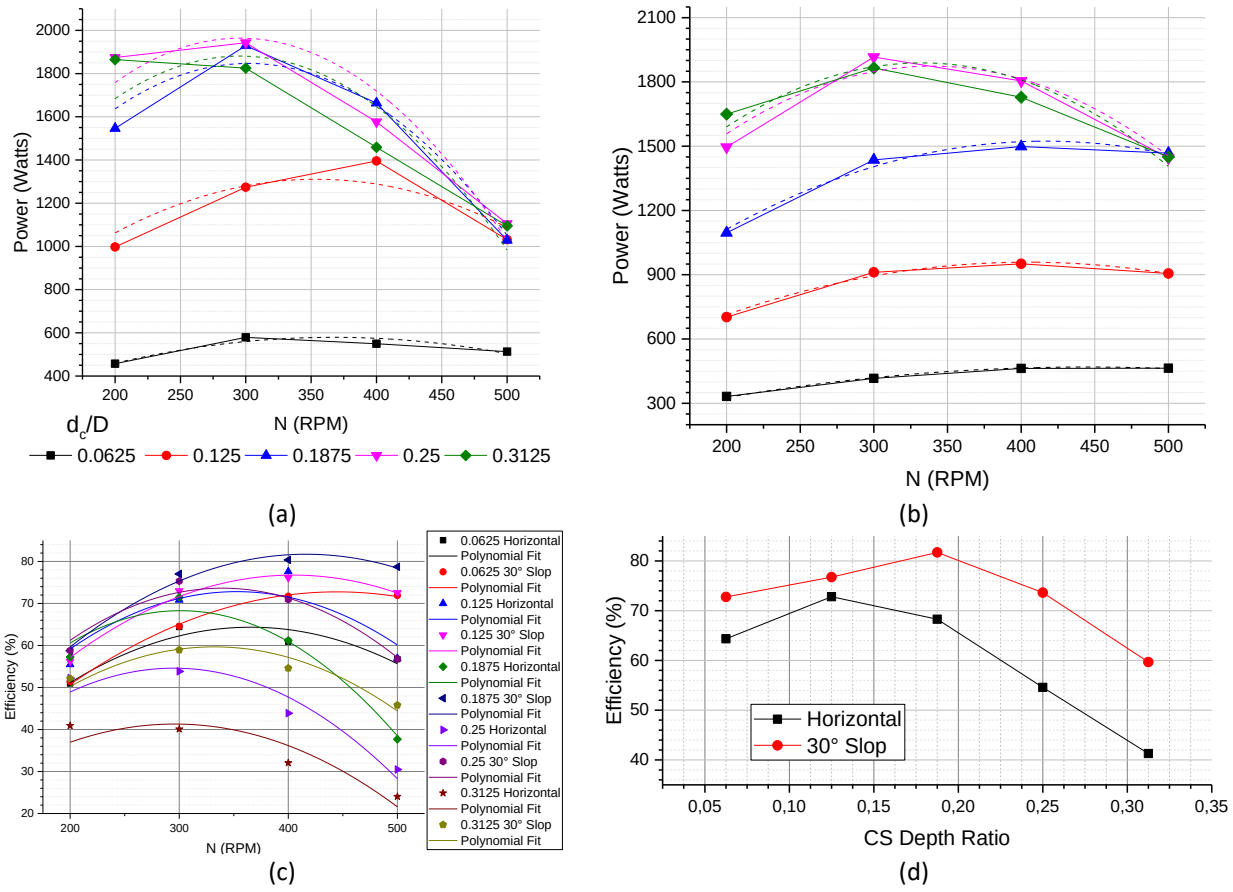

Fig. 4. The CFT performance; (a) Horizontal case power, (b) 30° slop case power, (c) All case efficiency, and (d) Optimum CS depth ratio

4. Discussions

The first thing that should be discussed more deeply is how relevant the simulation results in this study are to the findings in prior studies. The discussion should answer the question of how these simulation results could be said to be valid results. The following discussion is about some reasoning for the findings in this study with some theoretical approaches. Moreover, deeper data is provided to ensure the discussed reason is accountable and based on data.

4.1 The CFD Simulation Results Verification

This study compares the simulation results with the experiment data in a prior study to know how relevant the simulation results in this study are to the actual conditions [14]. The comparison visual can be seen in the graphic in Figure 5. The graphic shows that all three of the efficiency data have a peak condition at the range of maximum efficiency between 75% and 82%. Moreover, the graphic also shows that all three of the CFT performance curve has a maximum efficiency located in the range of $^{u}/_{V}$ between 0.48 and 0.52. These findings indicate that the CFT exhibit the same behaviour between the simulation and the experimental results, even with or without the nozzle and casing.

Some differences somehow are located at the higher value of $^{u}/_{V}$, while the nozzle-based CFT works tend to keep at an efficiency of more than 78%, the open-channel-based simulation results dramatically decrease efficiency, especially for horizontal channel conditions. The reasoning behind this finding is investigated in subchapter 4.2.

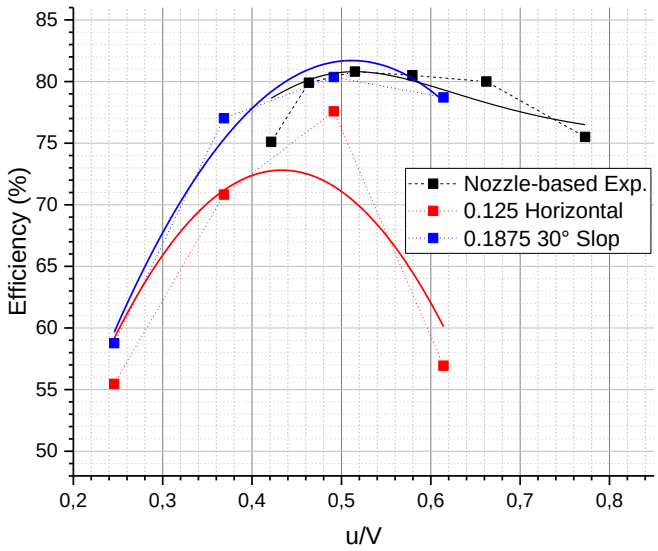

Fig. 5. Comparison between this study's CFD simulation results with a nozzle-based CFT experiment results

4.2 The Losses Analysis

One of the key differences between the open-channel-based and the nozzle-based CFT is the existence of the free surface of water flow incoming to the CFT. This condition makes the water flow come to the turbine freely and not be forced to enter the turbine. Thus, in some conditions, when the channel depth is too deep, or the rotational speed increases and disturbs the incoming water flow due to the centrifugal force, the water only flows over the CFT. These phenomena can be seen with the volume fraction visualization of water inside Figure 6. It can be seen in the $^{d_c}/_{D} = 0.1875$

condition for the horizontal flow and the $^{d_c}/_{D} = 0.3125$ in 30° slop flow, some water (red colour band) only flowed over the turbine without entering it. This condition leads to a significant loss to the OCF-CFT, named the potential loss in this study. Furthermore, the amount and the portion of this type of loss to the total loss are plotted on the graphic inside Figure 7.

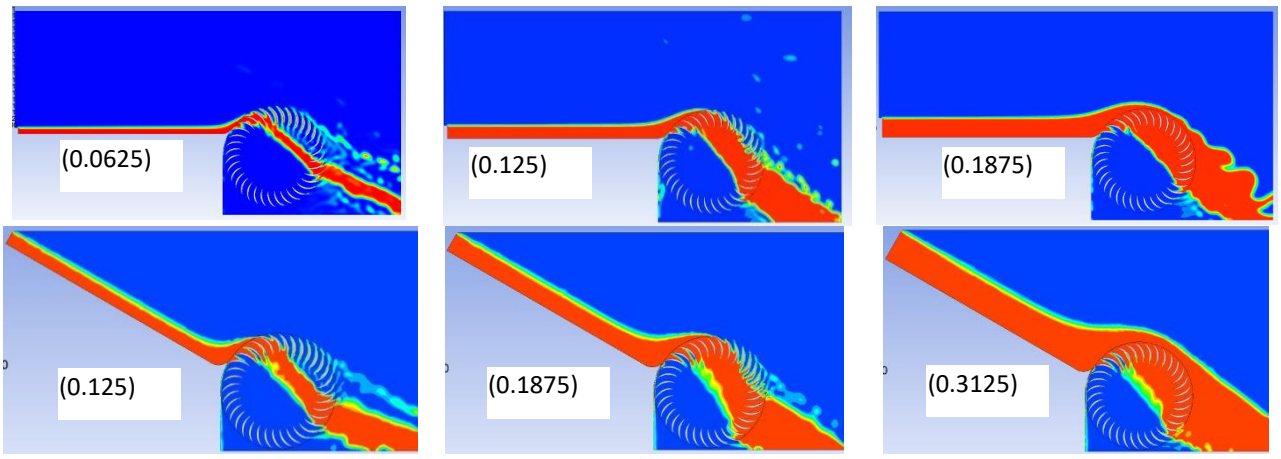

Fig. 6. The water volume fraction at 400 RPM for various $^{d_c}/_{D}$ condition in horizontal and 30° slop cases

It can be seen from Figure 7 that at the same $^{d_c}/_{D}$ ratio, a higher rotational speed leads to a higher potential loss in horizontal and 30° slop spillways. However, the horizontal channel OCF tends to have a higher amount and portion of the potential loss at the same condition than a 30° slop. That is why the optimum CS-Depth Ratio value on the horizontal channel is lower than a 30° slop.

Figure 7 also indicates that the portion of other loss out of the potential loss declined along with the rotational speed increment. A significant decrease of the non-potential loss occurred in 300 RPM with $^{d_c}/_{D} = 0.25$ condition on both horizontal and 30° slop cases. The phenomena that occurred led this point to the maximum power output of OCF-CFT in both cases. The deeper analysis in this study finds that the non-potential loss is mainly due to the variation in the angle of attack (α) between the water flow and the blade's tangential velocity. The optimum α for CFT has already been found at 22° by concluding the results of two studies by Aziz and Desai [23] in 1993 and Aziz and Totapally [24] in 1994. Moreover, De Andrade *et al.,* [25] have investigated the α variation in nozzle-based CFT. The velocity vector visualization and the angle of attack distribution in $^{d_c}/_{D} = 0.25$ condition for rotational speeds at 200 RPM, 300 RPM and 500 RPM in both cases displayed in Figure 8.

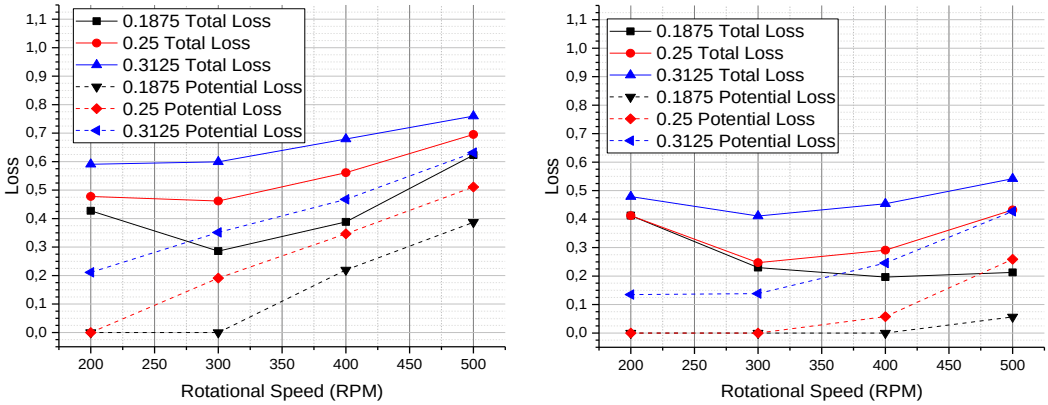

Fig. 7. The total and potential losses in OCF-CFT: (a) Horizontal channel; (b) 30° slop channel

The graph in Figure 8 shows that at the rotation speed of 300 RPM, the angle of attack variation is more stable than at 200 RPM and 500 RPM at rotational speed. Moreover, the 30° slop channel creates a higher α than a horizontal one. That causes the power of $^{d_c}/_{D} = 0.25$ horizontal OCF-CFT at 300 RPM is higher than the other configuration. The reasoning for this condition is that the higher value of α indicates that the water momentum is more likely to strike the back of the blades instead of their front face. The same reasoning also connects the fact that the gap between the total loss and the potential loss at 500 RPM condition is smaller than 200 RPM while the 500 RPM speed gives a lower value of α based on data in the graph.

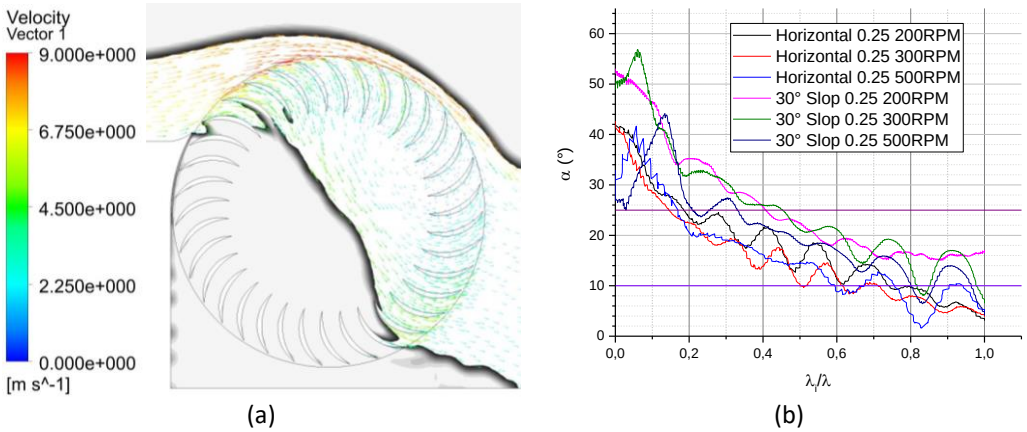

Fig. 8. a. The $^{d_c}/_{D} = 0.25$ @ 300RPM water velocity vector; b. the α value variation

5. Conclusion

The OCF-CFT have been tested in this study and give outstanding performance with a maximum efficiency of about 80.4% at the 30° spillway slop condition. Moreover, the horizontal flow OCF-CFT also provides a competitive performance with 77% maximum efficiency. These results show that the OCF-CFT is competitive with the nozzle-based CFT with a more straightforward design and lower manufacturing cost.

Acknowledgement
This paper's author would like to thank the Artificial Intelligence, Big Data, and Computing Technology (AIBDTK) Programme House, Electronic and Informatics Research Organization (OREI),

National Research and Innovation Agency (BRIN) for supporting this study on Grants No. B-1832/II.5.4/KU.01.03/4/2023.

References

[1] Duflo, Esther, and Rohini Pande. "Dams." *The Quarterly Journal of Economics* 122, no. 2 (2007): 601-646. https://doi.org/10.1162/qjec.122.2.601

[2] Altinbilek, Doğan. "The role of dams in development." *Water Science and Technology* 45, no. 8 (2002): 169-180. https://doi.org/10.2166/wst.2002.0172

[3] Chanson, Hubert. "Self-aerated flows on chutes and spillways." *Journal of Hydraulic Engineering* 119, no. 2 (1993): 220-243. https://doi.org/10.1061/(ASCE)0733-9429(1993)119:2(220)

[4] Müller, Gerald, and Klemens Kauppert. "Old watermills-Britain's new source of energy?." In *Proceedings of the Institution of Civil Engineers-Civil Engineering*, vol. 150, no. 4, pp. 178-186. Thomas Telford Ltd, 2002. https://doi.org/10.1680/cien.2002.150.4.178

[5] Gotoh, M., H. Kowata, T. Okuyama, and S. Katayama. "Damming-up effect of a current water wheel set in a rectangular channel." In *World Renewable Energy Congress VI*, pp. 1615-1618. Pergamon, 2000. https://doi.org/10.1016/B978-008043865-8/50333-0

[6] Budiarso, Budiarso, Warjito Warjito, Jonathan Sahat, Dendy Adanta, and Aji Putro Prakoso. "Influence of bucket shape and kinetic energy on breastshot waterwheel performance." In *2018 4th International Conference on Science and Technology (ICST)*, pp. 1-6. IEEE, 2018. https://doi.org/10.1109/ICSTC.2018.8528692

[7] Adanta, Dendy, Muhamad Agil Fadhel Kurnianto, and Sanjaya B. S. Nasution. "Effect of the number of blades on undershot waterwheel performance for straight blades." In *IOP Conference Series: Earth and Environmental Science*, vol. 431, no. 1, p. 012024. IOP Publishing, 2020. https://doi.org/10.1088/1755-1315/431/1/012024

[8] Williamson, Sam J., Bernard H. Stark, and Julian D. Booker. "Low head pico hydro turbine selection using a multi-criteria analysis." *Renewable Energy* 61 (2014): 43-50. https://doi.org/10.1016/j.renene.2012.06.020

[9] Mockmore, Charles Arthur, and Fred Merryfield. "The Bank Water Turbine." *Bulletin Series No. 25. Oregon State College, Corvallis* (1949).

[10] Prakoso, Aji Putro, Wirawan Piseno, Damawidjaya Bisono, Deny Bayu Saefudin, Ahmad Fudholi, and Fikri Nur Rohman. "Comparative Study on NACA-9405, NACA-9503 and NACA-9506 Airfoil Profiled Blade Open-Channel Flow Cross-Flow Turbine." *Public Research Journal of Engineering, Data Technology and Computer Science* 1, no. 1 (2023): 10-19.

[11] Prakoso, Aji Putro, Deny Bayu Saefudin, Damawidjaya Biksono, Dendy Adanta, and Reza Arvian. "The development of nozzle-less pico hydro Banki turbine: Fundamental theory and numerical simulations." In *AIP Conference Proceedings*, vol. 2689, no. 1. AIP Publishing, 2023. https://doi.org/10.1063/5.0114222

[12] Sammartano, Vincenzo, Costanza Aricò, Armando Carravetta, Oreste Fecarotta, and Tullio Tucciarelli. "Banki-Michell optimal design by computational fluid dynamics testing and hydrodynamic analysis." *Energies* 6, no. 5 (2013): 2362-2385. https://doi.org/10.3390/en6052362

[13] Siswantara, Ahmad Indra, Budiarso Budiarso, Aji Putro Prakoso, Gun Gun R. Gunadi, Warjito Warjito, and Dendy Adanta. "Assessment of turbulence model for cross-flow pico hydro turbine numerical simulation." *CFD Letters* 10, no. 2 (2018): 38-48.

[14] Sammartano, Vincenzo, Gabriele Morreale, Marco Sinagra, and Tullio Tucciarelli. "Numerical and experimental investigation of a cross-flow water turbine." *Journal of Hydraulic Research* 54, no. 3 (2016): 321-331. https://doi.org/10.1080/00221686.2016.1147500

[15] Adanta, Dendy, Dewi Puspita Sari, Nura Muaz Muhammad, and Aji Putro Prakoso. "History of Utilization of The Computational Fluid Dynamics Method for Study Pico Hydro Type Cross-Flow." *Indonesian Journal of Engineering and Science* 2, no. 1 (2021): 017-024. https://doi.org/10.51630/ijes.v2i1.11

[16] Adanta, Dendy. "Computational Analysis of Flow Field on Cross-Flow Hydro Turbines." *Engineering Letters* 29, no. 1 (2020).

[17] Rajaratnam, N., and D. Muralidhar. "Pressure and velocity distribution for sharp-crested weirs." *Journal of Hydraulic Research* 9, no. 2 (1971): 241-248. https://doi.org/10.1080/00221687109500348

[18] Cain, Paul, and Ian R. Wood. "Measurements of self-aerated flow on a spillway." *Journal of the Hydraulics Division* 107, no. 11 (1981): 1425-1444. https://doi.org/10.1061/JYCEAJ.0005761

[19] Richards, Shane A. "Completed Richardson extrapolation in space and time." *Communications in Numerical Methods in Engineering* 13, no. 7 (1997): 573-582. https://doi.org/10.1002/(SICI)1099-0887(199707)13:7<573::AID-CNM84>3.0.CO;2-6

[20] Prakoso, Aji Putro, Warjito Warjito, Ahmad Indra Siswantara, Budiarso Budiarso, and Dendy Adanta. "Comparison Between 6-DOF UDF and Moving Mesh Approaches in CFD Methods for Predicting Cross-Flow PicoHydro Turbine Performance." *CFD Letters* 11, no. 6 (2019): 86-96.

[21] Adanta, Dendy, Budiarso Budiarso, Warjito Warjito, and Ahmad Indra Siswantara. "Assessment of turbulence modelling for numerical simulations into pico hydro turbine." *Journal of Advanced Research in Fluid Mechanics and Thermal Sciences* 46, no. 1 (2018): 21-31.

[22] Daryus, Asyari, Ahmad Indra Siswantara, Steven Darmawan, Gun Gun R. Gunadi, and Rovida Camalia. "CFD simulation of turbulent flows in proto X-3 bioenergy micro gas turbine combustor using std k-ε and rng k-ε model for green building application." *International Journal of Technology* 7, no. 2 (2016): 204-211. https://doi.org/10.14716/ijtech.v7i2.2978

[23] Aziz, N. M., and V. R. Desai. "A laboratory study to improve the efficiency of cross-flow turbines (Engineering Report 1W-91)." *Department of Civil Engineering, Clemson University, Clemson, SC, USA* (1993).

[24] Aziz, N. M., and H. G. S. Totapally. "Design Parameter Refinement for Improved Cross Flow Turbine Performance." *Engineering Report* (1994).

[25] De Andrade, Jesús, Christian Curiel, Frank Kenyery, Orlando Aguillón, Auristela Vásquez, and Miguel Asuaje. "Numerical investigation of the internal flow in a Banki turbine." *International Journal of Rotating Machinery* 2011 (2011). https://doi.org/10.1155/2011/841214